Journal of Microscopy, Vol. 202, Pt 3, June 2001, pp. 451–456.
Received 30 October 2000; accepted 28 February 2001

SHORT COMMUNICATION

Improved spatial discrimination of protein reaction states in cells by global analysis and deconvolution of fluorescence lifetime imaging microscopy data

P. J. VERVEER*, A. SQUIRE* & P. I. H. BASTIAENS*†
**Cell Biology and Cell Biophysics Program, European Molecular Biology Laboratory, Meyerhofstraße 1, D-69117 Heidelberg, Germany*
†Cell Biophysics Laboratory, Imperial Cancer Research Fund, 44 Lincoln's Inn Fields, London, WC2A 3PX, U.K.

Key words. GFP, green fluorescent protein, FLIM, fluorescence resonance energy transfer, FRET, image restoration, protein interactions.

Summary

The deconvolution of fluorescence lifetime imaging microscopy (FLIM) data that were processed with global analysis techniques is described. Global analysis of FLIM data enables the determination of relative numbers of molecules in different protein reaction states on a pixel-by-pixel basis in cells. The three-dimensional fluorescence distributions of each protein state can then be calculated and deconvolved. High-resolution maps of the relative concentrations of each state are then obtained from the deconvolved images. We applied these techniques to quantitatively image the phosphorylation state of ErbB1 receptors tagged with green fluorescent protein in MCF7 cells.

Introduction

Fluorescence lifetime imaging microscopy (FLIM) is an emerging technique that has found many applications of physiological relevance in the biological sciences (Gadella *et al.*, 1993; Lakowicz *et al.*, 1993; Szmancinski & Lakowicz, 1995; Bastiaens & Jovin, 1996; Bastiaens & Squire, 1999; Ng *et al.*, 1999; Wouters & Bastiaens, 1999; Verveer *et al.*, 2000b). Of particular interest is the possibility to measure fluorescence resonance energy transfer (FRET) between a donor and an acceptor fluorophore, which enables measurement of the proximity of macromolecules on a nanometre scale (Bastiaens & Squire, 1999). This makes it possible to detect protein interactions in each resolvable element of the microscope.

Correspondence: P. I. H. Bastiaens. Tel.:. + 49 6221387 407; fax: + 49 6221387 242; e-mail: Philippe.Bastiaens@embl-heidelberg.de

The frequency domain FLIM imaging technique was recently enhanced using global analysis methods, enabling the quantitative determination of the relative concentrations of molecules (Verveer *et al.*, 2000a) and populations of molecular states (Verveer *et al.*, 2000b). The global analysis technique takes a different approach to extract information about the decay kinetics of the sample than the conventional method for analysing single frequency FLIM data. In the conventional approach a single lifetime value is calculated in each pixel, which represents a weighted average of the fluorescence lifetimes of all molecular species that are present. If more than one species of molecule is present, they cannot be resolved quantitatively, although changes in the relative quantities can be detected by monitoring changes in the apparent lifetime. In addition, the measured lifetimes are strongly influenced by blurring with the point-spread-function (PSF) of the microscope, as it determines the size of the volume element over which the lifetimes are weighted (Squire & Bastiaens, 1999). Thus, for a sample composed of two or more molecular species with different fluorescence lifetimes, the accuracy of the lifetime estimation is influenced by the resolution of the imaging system, which is generally not desirable, and especially a problem in a widefield set-up. The global analysis approach uses a priori knowledge about the biochemical system under study to calculate the fluorescence lifetimes of all species in the sample, and the populations (fractional amounts) of molecules in all pixels. In this paper we use FLIM with global analysis to quantitatively study FRET that arises when a donor and an acceptor molecule are brought into proximity upon the formation of a protein complex. Because the spatial configuration of the complex is fixed upon

binding, it can be reasonably assumed that the distribution of lifetimes of the donor in the complex can, within the resolution of the FLIM system, be approximated with a single spatially invariant value. Clearly, it must be verified that effects of the cellular environment, other than FRET, can be neglected. Unlike a conventional analysis, a global analysis gives quantitative information, and additionally, the fluorescence lifetime estimations obtained are unaffected by the resolution of the imaging system. Multiplication of the population maps with the steady-state fluorescence image yields the fluorescence intensity emitted by each species. Although blurring by the PSF does not affect the estimated lifetimes, the fluorescence of each species is subject to this blurring and therefore the population maps returned by the global analysis are affected.

In previous work, we demonstrated that it is possible to improve temporal and spatial resolution by applying deconvolution techniques to the Fourier coefficients calculated from FLIM data, prior to a conventional lifetime analysis (Squire & Bastiaens, 1999). In this short communication we use a different approach where the fluorescence of the different molecular species is first separated by global analysis and then deconvolved. We show that this leads to a marked improvement in the spatial resolution of the population images that are calculated from the deconvolved fluorescence images. To demonstrate its utility in a biological application, we imaged the biochemical state (phosphorylated or unphosphorylated) of the plasma membrane-bound epidermal growth factor receptor ErbB1, fused to the green fluorescent protein EGFP (Wouters & Bastiaens, 1999), by measuring FRET between ErbB1-GFP and Cy3 labelled antiphosphotyrosine antibody (Cy3/PY72) (see also Verveer *et al.*, 2000b).

Materials and methods

FLIM microscopy

The FLIM set-up used in this work has been described in detail before (Squire & Bastiaens, 1999). Briefly, the light of an argon/krypton laser with a 488 nm wavelength was modulated using a standing wave acousto-optic modulator (Intra-Action Corp., Belwood, U.S.A.) at a frequency of 80.244 MHz. The spatial and temporal coherence properties of the laser beam were removed using a rotating ground-glass disc, before directing the light into the epi-illumination port of an inverted microscope (Zeiss Axiovert 135TV, Carl Zeiss, Welwyn Garden City, U.K.). Fluorescent light from the sample was collected with a 100 × 1.4 NA oil immersion lens, a 505 LP (Chroma Technology Corp., Brattleboro, U.S.A.) dichroic in combination with a 514/10 emission filter (Delta Light & Optics, Lyngby, Denmark), an image intensifier (Hamamatsu C5825, Hamamatsu Photonics UK Ltd, Welwyn Garden City, U.K.) gain modulated at 80.244 MHz and imaged to a CCD camera (Photometrics Quantix, Roper Scientific, Marlow, U.K.) with a 0.5 × magnification. The resulting signal is dependent on the phase-difference between the modulation of the laser intensity and the gain of the microchannel plate detector (homodyne detection) and was sampled by acquiring four images with the phase of the intensifier modulation shifted over 90° steps.

PSF measurement

A PSF was measured while modulating the image intensifier gain, but without modulation of the laser light. A 50-fold dilution of TetraSpeck (Molecular Probes, Leiden, The Netherlands) fluorescent blue/green/orange/dark red 0.2 μm beads was pipetted onto a poly L-lysine-coated coverslip and left to dry. The coverslip was placed onto a drop of mowiol on a microscope slide and left overnight in the refrigerator. Stacks of 64 images were obtained at 0.25 μm intervals with a 4-s exposure time for each image. Three fields were imaged for a total of 15 beads. Each stack was imaged twice, once moving the focus downwards and once moving it upwards. From the stacks, volumes containing the individual beads were extracted and registered by shifting their centre of mass to a common origin. From a region in the stack that did not contain any beads, the background value was estimated and subtracted. The orientation of the PSFs was matched by mirroring the bead images that were acquired while moving the focus up. The PSF was obtained by adding all resulting bead images to improve the signal-to-noise ratio. Because each bead was imaged twice, once moving up and once moving down in the axial direction, addition of all images resulted in a first order correction for photobleaching.

Cell measurements

MCF7 cells expressing ErbB1-GFP receptors were stimulated for 5 min with soluble epidermal growth factor (EGF) and prepared as described in Wouters & Bastiaens (1999). The samples were imaged using the same microscope parameters as described above, but with a 2 × 2 binning of the CCD camera. A stack of 40 images was obtained at 0.5 μm intervals. The exposure time for each image was 150 ms, and no appreciable photobleaching was observed over each phase-sequence of four images. Photobleaching over the time-course of acquisition of the complete three-dimensional stack was extensive, and was compensated for numerically as described below.

FLIM data analysis

Four sections from the middle of the stack of FLIM sequences were extracted and global analysis was applied

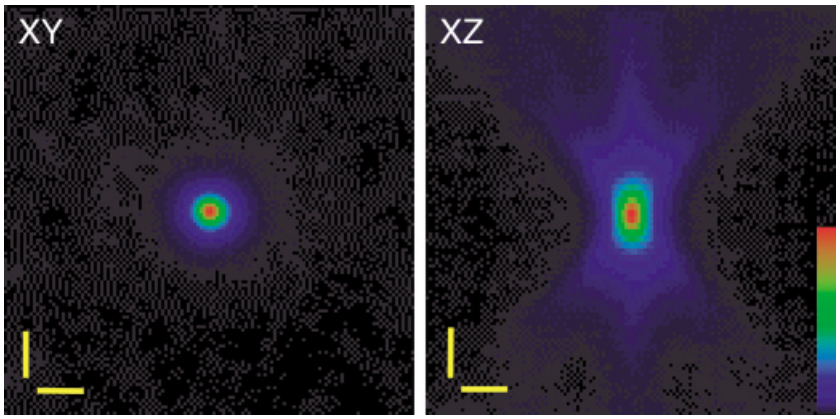

Fig. 1. Point spread function of the FLIM system. Lateral (XY) and axial (XZ) slices through the middle of the PSF are shown. Scale bars are 2 μm. Colour bar is in arbitrary units.

as described by Verveer *et al.* (2000a, 2000b), assuming two different states with distinct spatially invariant lifetime values. The global analysis was only performed using pixels with a sufficient fluorescent signal in a few sections from the middle of the stack. For this reason the populations were recalculated for all pixels in the stack with a linear estimation (see Verveer *et al.*, 2000a) using the lifetime values obtained in the global analysis. The total fluorescence (obtained for each section in the stack by adding all images in the FLIM sequence) was multiplied with the population maps of each species to obtain their three-dimensional spatially resolved fluorescence intensities. These were corrected individually for photobleaching by renormalizing the total intensity in each section of the stack to be equal to that of the first section. This correction is based upon the assumption that the total flux of light through the sample is constant, which is approximately true for small regions in the field of view of a wide-field microscope. It is essential that the fluorescence for each state is corrected separately, as the difference in the lifetimes of the two species results in a different photobleaching rate for the individual stacks. The image stacks were then deconvolved using an accelerated iterative constrained Tikhonov–Miller (ICTM) algorithm (Verveer & Jovin, 1997). Deconvolved population images were obtained by dividing the deconvolved fluorescence images of the phosphorylated and unphosphorylated species by the deconvolved total fluorescence after masking out low intensity values to prevent amplification of noise by the division operation. Population images were then renormalized by their corresponding lifetime values to correct for the difference in the quantum yields (see Verveer *et al.*, 2000a).

Results

Figure 1 shows the PSF of the FLIM instrument, which is substantially larger than usual for a widefield fluorescence microscope. This is because of the frequency-dependent loss of spatial resolution introduced by the image intensifier (Hamamatsu-Photonics-K.K., 1995). Clearly it is essential to use a carefully measured PSF, obtained at the correct frequency of modulation of the image intensifier.

We applied global analysis techniques to obtain population images of phosphorylated and unphosphorylated ErbB1 receptors in MCF7 cells. To confirm that the decay of ErbB1-GFP can be assumed to be mono-exponential in our global analysis, we used a conventional analysis to determine phase and modulation lifetimes with their errors from samples that were stimulated for various times with EGF, but not incubated with antibody. The average values over several 2D images (835577 pixels in total) for phase and modulation estimations were 2.05 ± 0.14 and 2.20 ± 0.14 ns (errors are standard deviations from an error analysis). Thus, the difference in the phase and modulation estimations is not significant at this modulation frequency. Therefore it is reasonable to assume that contributions from any additional components are negligible at this frequency, and a single exponential model for ErbB1-GFP can be applied in the global analysis. The spatial variation in the ErbB1-GFP lifetime value can be characterized by the standard deviations in the phase and modulation lifetime estimations, as estimated from all pixels, which were equal to 0.11 and 0.09 ns, respectively. Thus, there are no significant spatial variations compared to the estimated errors of the lifetimes. Therefore, environmental influences have no substantial effects on the lifetime of the donor. Also the lifetime of the donor was independent of the duration of EGF stimulation, therefore showing that there are no ligand-induced effects on the lifetime of the donor alone. Thus, any significant lifetime change in the presence of the antibody can be attributed to FRET.

The phosphorylation state of the receptors can be detected by measuring the decrease in lifetime of ErbB1-GFP when FRET occurs between the GFP donor and the Cy3/PY72 acceptor. The fluorescence originating from each species (phosphorylated or unphosphorylated) can then be separated and deconvolved. The lifetime values that were found from the three-dimensional FLIM data measured on samples that were incubated with antibody were 0.81 and 2.22 ns, in good agreement with earlier results (Verveer

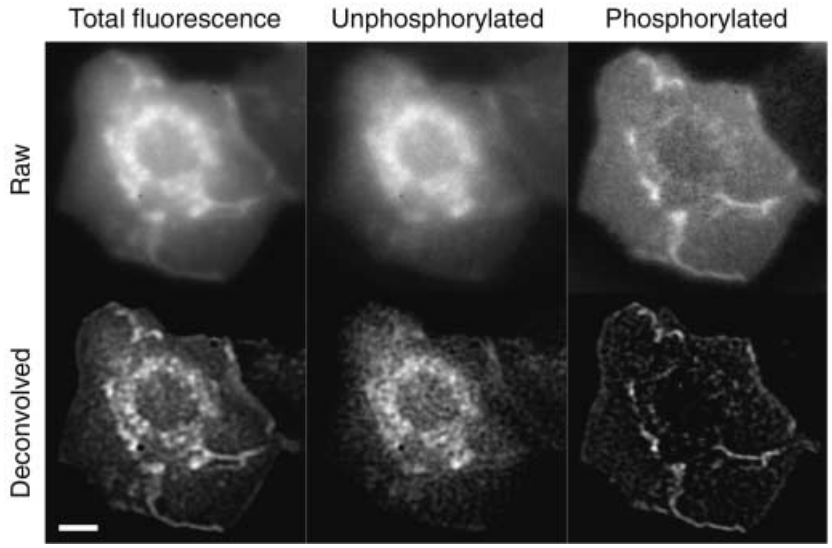

Fig. 2. Total fluorescence and the fluorescence from unphosphorylated and phosphorylated ErbB1-GFP receptors before and after deconvolution. The summations of 10 consecutive sections through the middle of the cell are shown. Scale bar is 10 μm.

et al., 2000b), and the ErbB1-GFP lifetime value found from samples without Cy3/PY72.

Figure 2 shows the total fluorescence, and the fluorescence intensity originating from unphosphorylated and phosphorylated ErbB1-GFP, before and after deconvolution using the measured PSF of Fig. 1. A clear separation is obtained between phosphorylated (active) ErbB1 receptors on the plasma membrane and unphosphorylated (inactive) material on membranes in the cytoplasm. After deconvolution out-of-focus fluorescence is removed and resolution is improved. From the deconvolved images, it can clearly be observed that most of the fluorescence intensity in the cell originates from unphosphorylated receptors inside the cytoplasm. Note the ruffles on top of

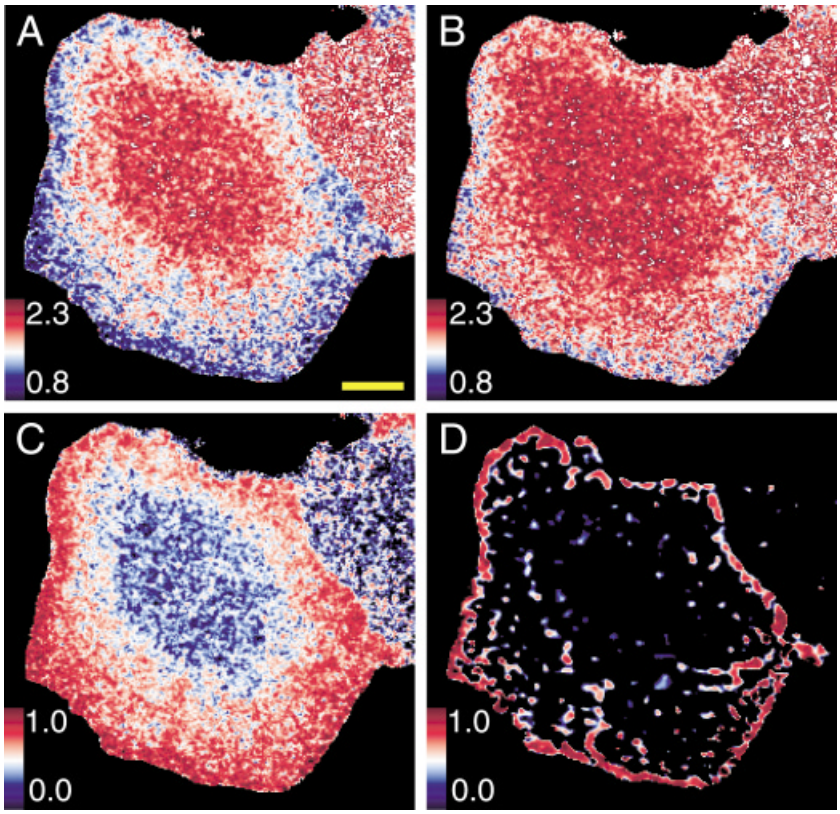

Fig. 3. Imaging FRET in a single section through a MCF7 cell. (A) Conventional calculation of the apparent lifetimes (ns) from the estimated phase shifts. (B) Conventional calculation of the apparent lifetimes (ns) from the estimated demodulations. (C) Populations of phosphorylated ErbB1 receptor calculated from the fluorescence intensities of each species before deconvolution. (D) Populations calculated after deconvolution. Scale bar is 10 μm.

the cell that appear only in the images of the phosphorylated receptor, indicating that these ruffles are rich in activated ErbB1-receptors. These ruffles are induced upon EGF stimulation and arise from the formation of lamellipodial extensions that are involved in cell motility (Wells *et al.*, 1998).

Figure 3 shows the apparent lifetime values calculated using the conventional method from the estimated phase-shifts (Fig. 3A) and demodulations (Fig. 3B) in a single section through the middle of the cell. Because the apparent lifetime value is a weighted average, depending on the true spatially invariant lifetime values and the spatially varying populations, a drop in the apparent lifetime value is seen where FRET occurs. However, no quantitative information about the relative numbers of receptors is available in this image. This information is available in the result of the global analysis, also shown in Fig. 3.

The significance of the deconvolution becomes clear if the populations of phosphorylated receptors in a single section are inspected (Figs 3C and D). Before deconvolution it appears that a significant fraction of phosphorylated receptor is present not only on the plasma membrane, but also deeper inside the cytoplasm (Fig. 3C). However, after deconvolution, it is clear that the phosphorylated receptors are only present on the membrane, and not in the cytoplasm (Fig. 3D). Thus, the fluorescence inside the cell originates only from ErbB1-GFP in compartments that were not exposed to the extracellular stimulus, either *de novo* receptor in transit to the plasma membrane, or receptors participating in endocytosis prior to stimulation. Note also that the population values of phosphorylated receptor in the plasma membrane reach 100%, demonstrating that all receptors in the plasma membrane have reacted after ligand binding. The clear discrimination that was obtained between the distributions of ligand-activated receptor in the plasma membrane, and inactive receptor within compartments of the cytoplasm that cannot bind ligand (Figs 2 and 3), independently validates our approach.

Conclusions

Global analysis is a novel approach to analyse FLIM data in a quantitative manner, enabling the discrimination of protein reaction states on a pixel-by-pixel basis, and simultaneously obtaining estimations of the lifetime of each species that are unaffected by the PSF. The resulting population images are still subject to blurring by the PSF, but as the three-dimensional fluorescence distribution of each molecular species or state can now be calculated, this can be easily corrected using a standard deconvolution approach as shown in this paper. This approach to deconvolution of FLIM data is substantially different from the approach described earlier by Squire & Bastiaens (1999), where the Fourier coefficients of the FLIM data were deconvolved prior to calculating the apparent lifetimes. The approach described here estimates the true lifetimes before deconvolution from regions with sufficient intensity. The fluorescence intensity of each species is subsequently calculated in each pixel of the stack after which a deconvolution is applied to each species separately. An advantage of this approach is that prior to deconvolution the fluorescence of each species can be corrected individually for photobleaching. It is difficult to apply such a photobleaching correction prior to global analysis when the composition of the sample is still unknown, because each species photobleaches with a different rate.

These methods are not limited to widefield FLIM data, but should be applicable to other types of lifetime microscopy, including confocal setups. Optical sectioning techniques, such as confocal microscopy, have been applied in FLIM and significantly reduce out-of-focus blurring (Buurman *et al.*, 1992; Draaijer *et al.*, 1995; Carlsson & Liljeborg, 1997), but are limited by speed and sensitivity constraints. One solution may be the application of spinning disk technology, in particular by employing microlens disks. This approach was taken by Straub & Hell (1998) employing a rotating microlens disk and a gated, intensified CCD camera. Other novel optical sectioning approaches are emerging that may be used to adapt a widefield FLIM microscope (Hanley *et al.*, 1999; Neil *et al.*, 2000), combining the advantages of widefield and confocal set-ups. Recently, structured illumination was used to successfully obtain sectioned FLIM images (Cole *et al.*, 2000). Even though confocal or alternative set-ups provide inherent sectioning capability, it should still be possible to further improve the resolution of FLIM data sets taken with such instruments using the methods described in this paper.

Acknowledgements

P.J.V. was supported by a long-term fellowship from the European Molecular Biology Organization (EMBO). We thank Dr F. S. Wouters for providing the MCF7 samples. We are indebted to one of the reviewers for his or her constructive and critical comments.

References

Bastiaens, P.I.H. & Jovin, T.M. (1996) Microspectroscopic imaging tracks the intracellular processing of a signal transduction protein: fluorescent-labeled protein kinase C βI. *Proc. Natl. Acad. Sci.* **93**, 8407–8412.

Bastiaens, P.I.H. & Squire, A. (1999) Fluorescence lifetime imaging microscopy: spatial resolution of biochemical processes in the cell. *Trends Cell Biol.* **9**, 48–52.

Buurman, E.P., Sanders, R., Draaijer, A., Gerritsen, H.C., van Veen, J.J.F., Houpt, P.M. & Levine, Y.K. (1992) Fluorescence lifetime

imaging using a confocal laser scanning microscope. *Scanning*, **14**, 155–159.

Carlsson, K. & Liljeborg, A. (1997) Confocal fluorescence microscopy using spectral and lifetime information to simultaneously record four fluorophores with high channel separation. *J. Microsc.* **185**, 37–46.

Cole, M.J., Siegel, J., Webb, S.E.D., Jones, R., Dowling, K., French, P.M.W., Lever, M.J., Sucharov, L.O.D., Neil, M.A.A., Juškaitis, R. & Wilson, T. (2000) Whole-field optically sectioned fluorescence lifetime imaging. *Opt. Lett.* **25**, 1361–1363.

Draaijer, A., Sanders, R. & Gerritsen, H.C. (1995) Fluorescence lifetime imaging, a new tool in confocal microscopy. *Handbook of Biological Confocal Microscopy.* 2nd edn (ed. by J. B. Pawley), pp. 491–505. Plenum Press, New York.

Gadella, T.W. Jr, Jovin, T.M. & Clegg, R.M. (1993) Fluorescence lifetime imaging microscopy (FLIM) – spatial resolution of microstructures on the nanosecond time-scale. *Biophys. Chem.* **48**, 221–239.

Hanley, Q.S., Verveer, P.J., Gemkow, M.J. & Arndt-Jovin, D.J. (1999) An optical sectioning programmable array microscope implemented with a digital micromirror device. *J. Microsc.* **196**, 317–331.

Lakowicz, J.R., Nowaczyk, H.S. & Johnson, M.L. (1993) Fluorescence lifetime imaging of free and protein-bound NADH. *Proc. Natl. Acad. Sci.* **89**, 1271–1275.

Neil, M.A.A., Squire, A., Juškaitis, R., Bastiaens, P.I.H. & Wilson, T. (2000) Wide-field optically sectioning fluorescence microscopy with laser illumination. *J. Microsc.* **197**, 1–4.

Ng, T., Squire, A., Hansra, G., Bornancin, F., Prevostel, C., Hanby, A., Harris, W., Barnes, D., Schmidt, S., Mellor, H., Bastiaens, P.I.H. & Parker, P.J. (1999) Imaging protein kinase Cα activation in cells. *Science*, **283**, 2085–2089.

Squire, A. & Bastiaens, P.I.H. (1999) Three dimensional image restoration in fluorescence lifetime imaging microscopy. *J. Microsc.* **193**, 36–49.

Straub, M. & Hell, S.W. (1998) Fluorescence lifetime three-dimensional microscopy with picosecond precision using a multifocal multiphoton microscope. *Appl. Phys. Lett.* **73**, 1769–1771.

Szmancinski, H. & Lakowicz, J.R. (1995) Possibility of simultaneously measuring low and high-calcium concentrations using Fura-2 and lifetime-based sensing. *Cell Calcium*, **18**, 64–75.

Verveer, P.J. & Jovin, T.M. (1997) Acceleration of the ICTM image restoration algorithm. *J. Microsc.* **188**, 191–195.

Verveer, P.J., Squire, A. & Bastiaens, P.I.H. (2000a) Global analysis of fluorescence lifetime imaging microscopy data. *Biophys. J.* **78**, 2127–2137.

Verveer, P.J., Wouters, F.S., Reynolds, A.R. & Bastiaens, P.I.H. (2000b) Quantitative imaging of lateral ErbB1 receptor signal propagation in the plasma membrane. *Science*, **290**, 1567–1570.

Wells, A., Gupta, K., Chang, P., Swindle, S., Glading, A. & Shiraha, H. (1998) Epidermal growth factor receptor-mediated motility in fibroblasts. *Microsc. Res. Techn.* **43**, 395–411.

Wouters, F.S. & Bastiaens, P.I.H. (1999) Fluorescence lifetime imaging of receptor tyrosine kinase activity in cells. *Curr. Biol.* **9**, 1127–1130.